

# Geophysical Research Letters<sup>®</sup>

## RESEARCH LETTER

10.1029/2021GL095651

Keren Duer and Nimrod Gavriel contributed equally to this work.

### Key Points:

- Measurements from multiple instruments of the Juno mission are interpreted to reveal the meridional circulation beneath Jupiter's clouds
- 16 Jet-paired deep cells, extending from the cloud deck down to at least 240 bar, are revealed between latitudes 60°S and 60°N, driven by turbulence similar to Earth's Ferrel cells
- The findings are supported by modeling the advection of tracers due to the cells, showing agreement with NH<sub>3</sub> data

### Supporting Information:

Supporting Information may be found in the online version of this article.

### Correspondence to:









K. Duer,  
[keren.duer@weizmann.ac.il](mailto:keren.duer@weizmann.ac.il)

### Citation:

Duer, K., Gavriel, N., Galanti, E., Kaspi, Y., Fletcher, L. N., Guillot, T., et al. (2021). Evidence for multiple Ferrel-like cells on Jupiter. *Geophysical Research Letters*, 48, e2021GL095651. <https://doi.org/10.1029/2021GL095651>

Received 15 AUG 2021  
Accepted 8 OCT 2021

## Evidence for Multiple Ferrel-Like Cells on Jupiter

Keren Duer<sup>1</sup> , Nimrod Gavriel<sup>1</sup> , Eli Galanti<sup>1</sup> , Yohai Kaspi<sup>1</sup> , Leigh N. Fletcher<sup>2</sup> , Tristan Guillot<sup>3</sup> , Scott J. Bolton<sup>4</sup> , Steven M. Levin<sup>5</sup> , Sushil K. Atreya<sup>6</sup> , Davide Grassi<sup>7</sup> , Andrew P. Ingersoll<sup>8</sup> , Cheng Li<sup>6</sup> , Liming Li<sup>9</sup> , Jonathan I. Lunine<sup>10</sup> , Glenn S. Orton<sup>5</sup> , Fabiano A. Oyafuso<sup>5</sup> , and J. Hunter Waite<sup>4</sup> 

<sup>1</sup>Department of Earth and Planetary Sciences, Weizmann Institute of Science, Rehovot, Israel, <sup>2</sup>School of Physics and Astronomy, University of Leicester, Leicester, UK, <sup>3</sup>Université Côte d'Azur, OCA, Lagrange CNRS, Nice, France, <sup>4</sup>Southwest Research Institute, San Antonio, TX, USA, <sup>5</sup>Jet Propulsion Laboratory, California Institute of Technology, Pasadena, CA, USA, <sup>6</sup>Department of Climate and Space Sciences and Engineering, University of Michigan, Ann Arbor, MI, USA, <sup>7</sup>Istituto di Astrofisica e Planetologia Spaziali, INAF, Rome, Italy, <sup>8</sup>California Institute of Technology, Pasadena, CA, USA, <sup>9</sup>University of Houston, Houston, TX, USA, <sup>10</sup>Department of Astronomy, Cornell University, Ithaca, NY, USA

**Abstract** Jupiter's atmosphere is dominated by multiple jet streams which are strongly tied to its 3D atmospheric circulation. Lacking a rigid bottom boundary, several models exist for how the meridional circulation extends into the planetary interior. Here, we show, collecting evidence from multiple instruments of the Juno mission, the existence of midlatitudinal meridional circulation cells which are driven by turbulence, similar to the Ferrel cells on Earth. Different than Earth, which contains only one such cell in each hemisphere, the larger, faster rotating Jupiter can incorporate multiple cells. The cells form regions of upwelling and downwelling, which we show are clearly evident in Juno's microwave data between latitudes 60°S and 60°N. The existence of these cells is confirmed by reproducing the ammonia observations using a simplistic model. This study solves a long-standing puzzle regarding the nature of Jupiter's subcloud dynamics and provides evidence for eight cells in each Jovian hemisphere.

**Plain Language Summary** The cloud layer of Jupiter is divided into dark and bright bands that are shaped by strong east-west winds. Such winds in planetary atmospheres are thought to be tied with a meridional circulation. The Juno mission collected measurements of Jupiter's atmosphere at various wavelengths, which penetrate the cloud cover. Here, we provide evidence, using the Juno data, of eight deep Jovian circulation cells in each hemisphere encompassing the east-west winds, gaining energy from atmospheric waves, and extending at least to a depth of hundreds of kilometers. Different than Earth, which has only one analogous cell in each hemisphere, known as a Ferrel cell, Jupiter can contain more cells due to its larger size and faster spin. To support the presented evidence, we modeled how ammonia gas would spread under the influence of such cells and compared it to the Juno measurements. The presented results shed light on the unseen flow structure beneath Jupiter's clouds.

## 1. Introduction

Over the last few decades, spacecraft and ground-based observations have gathered data about Jupiter's atmosphere, including measurements of cloud reflectance (García-Melendo & Sánchez-Lavega, 2001), winds (Porco et al., 2003; Salyk et al., 2006; Tollefson et al., 2017), composition (Taylor et al., 2004), and lightning flashes (Little et al., 1999). Since 2016, the Juno spacecraft has provided unprecedented measurements that revealed new information on the deep dynamics of Jupiter (Bolton et al., 2017). Gravity science enabled an accurate mapping of Jupiter's gravitational field (Iess et al., 2018), resulting in the inference that the zonal jets penetrate ~3,000 km deep (Guillot et al., 2018; Kaspi et al., 2018), where they possibly decay due to magnetic drag (Dietrich & Jones, 2018; Kaspi et al., 2020; Liu et al., 2008) and may also require the presence of a stable layer (Christensen et al., 2020). The Jovian Infrared Auroral Mapper (JIRAM) provided measurements of tropospheric species distribution below the cloud level (Grassi et al., 2020). The Microwave Radiometer (MWR) measurements, inferred as brightness temperature ( $T_b$ ), revealed the deep ammonia abundance (Li et al., 2017; Oyafuso et al., 2020), as well as lightning at a frequency of 600 MHz (Brown et al., 2018). The combination of these observations allows the essential nature of Jupiter's deep overturning circulation to be revealed, as the flows associated with such circulation are directly related to cloud formation, temperature variations, lightning occurrences, tracer distributions, and turbulence.

Earth's atmosphere is commonly referred to as possessing a three-cell meridional structure in each hemisphere (Vallis, 2017), which can be recognized in the zonal-averaged velocities. Circulation cells of such nature are thought to prevail in the atmospheres of terrestrial planets (Read et al., 2018) and were observed, for example, on Mars (Lewis et al., 2007) and Venus (Limaye, 2007). On the terrestrial planets, the solid surface drag plays a part in maintaining the circulation in the cells. However, as the giant planets hold no such surface, the mere possibility of them possessing meridional circulation cells remained uncertain. Earth's midlatitudes are governed by the Ferrel cells, which are driven by atmospheric turbulence, creating regions of eddy momentum flux convergence at midlatitudes (Vallis, 2017). These cells accompany the midlatitude jets and are connected to the cloud structure in Earth's atmosphere.

The prominent banded structure at the cloud tops of Jupiter's atmosphere (Figure 1a) has been observed for centuries (Vasavada & Showman, 2005). These reflectivity contrasts are partially aligned (mainly at low latitudes; Ingersoll et al., 2000) with the belts and zones (Figure 1a), defined by the sign of the zonal-wind vorticity ( $\bar{\zeta} = -\partial\bar{u}/\partial y$  in Figure 1c, where  $u$  is the zonal velocity,  $y$  is in the meridional direction, and an overline represents a zonal mean). Voyager measurements suggested that the zones are associated with ascending motion, but this was limited to low latitudes due to its equatorial trajectory and to altitudes above 0.5 bar (Gierasch et al., 1986). The latitudinal profile of the zonal wind, calculated using cloud-tracking (García-Melendo & Sánchez-Lavega, 2001; Porco et al., 2003; Tollefson et al., 2017), reveals that the equatorial region is characterized by a strong eastward flow, while the midlatitudes exhibit alternating jets, spaced  $2 - 8^\circ$  apart in latitude (Figure 1b). The midlatitude jets are correlated with the eddy momentum flux convergence (Salyk et al., 2006) ( $-\partial(\overline{u'v'})/\partial y$  Figure 1d, where  $v$  is meridional velocity and an apostrophe represents deviations from the zonal mean, i.e., "eddy" terms), implying that the midlatitude jets are eddy-driven (Ingersoll et al., 2000; Young & Read, 2017), similar to the jets within Earth's Ferrel cells (Schneider, 2006; Vallis, 2017). To illustrate the relation between the jets and the eddies, regions of positive (negative) vorticity gradient,  $\partial\bar{\zeta}/\partial y = -\partial^2\bar{u}/\partial y^2$ , at midlatitudes, are marked by light red (blue) bands (Figure 1), where counterclockwise (clockwise) Ferrel-like circulation cells are expected in the northern hemisphere (NH). Similar circulations, but in opposite directions, apply for the southern hemisphere (SH). Evidence for vertical motion comes also from observations of lightning flashes (Brown et al., 2018; Little et al., 1999; Porco et al., 2003), suggesting updrafts in cyclonic belt regions (e.g., Figure 1e).

Additional information regarding Jupiter's deep atmosphere can be obtained by probing Jupiter's interior at microwave frequencies. Juno's MWR has six microwave channels (Janssen et al., 2017), each measuring the atmospheric  $T_b$  at a different depth (Bolton et al., 2017; Fletcher et al., 2021; Janssen et al., 2017; Oyafuso et al., 2020), and collectively covering the range between 0.7 and 240 bar (Figures 1g and 1h, see also Supporting Information S1).  $T_b$  measurements are affected by both ammonia abundance and temperature (and water in the case of the longest wavelengths; Fletcher et al., 2021; Li et al., 2017, 2020). If the latitudinal gradients of  $T_b$  were primarily driven by temperature changes, then thermal wind balance implies that the midlatitude jets strengthen from the cloud-deck to about  $\sim 8$  bar, and then decay slowly toward the interior (Fletcher et al., 2021). However, interpreting  $T_b$  as temperature would also imply that the equatorial wind double its magnitude below the cloud level (Bolton et al., 2017), which is inconsistent with gravity constraints (Duer et al., 2020). Thus, the latitudinal variation of  $T_b$  is probably governed by ammonia opacity, resulting in a map of ammonia abundance (Li et al., 2017), and implying that the zonal winds are nearly barotropic (Fletcher et al., 2021). The overall ammonia structure, supported also by earlier observations (de Pater et al., 2001), reveals stratification of ammonia with depth, although the mean ammonia profile changes the sign of its vertical gradient at the  $\sim 2 - 8$  bar region (de Pater et al., 2019; Giles et al., 2017; Li et al., 2017). The atmospheric depletion and stratification of ammonia are likely linked to small-scale storm activity (Guillot, Li, et al., 2020; Guillot, Stevenson, et al., 2020), where water-ammonia hail, forming around the 1-bar level, falls below the water-cloud base and releases ammonia and water at altitudes below 10 bar (Guillot, Stevenson, et al., 2020). Additional measurements of ammonia come from Juno's JIRAM, which evaluated the ammonia distribution at a depth of  $\sim 5 - 6$  bar (Grassi et al., 2010, 2020; Figure 1f), indicating, as the MWR measurements, that ammonia varies with latitude. These variations are the key observation for this study, as ammonia anomalies (deviations from the isobaric mean) can reveal details about Jupiter's overturning circulation (Duer et al., 2020; Fletcher et al., 2021; Ingersoll et al., 2017; Lee & Kaspi, 2021).

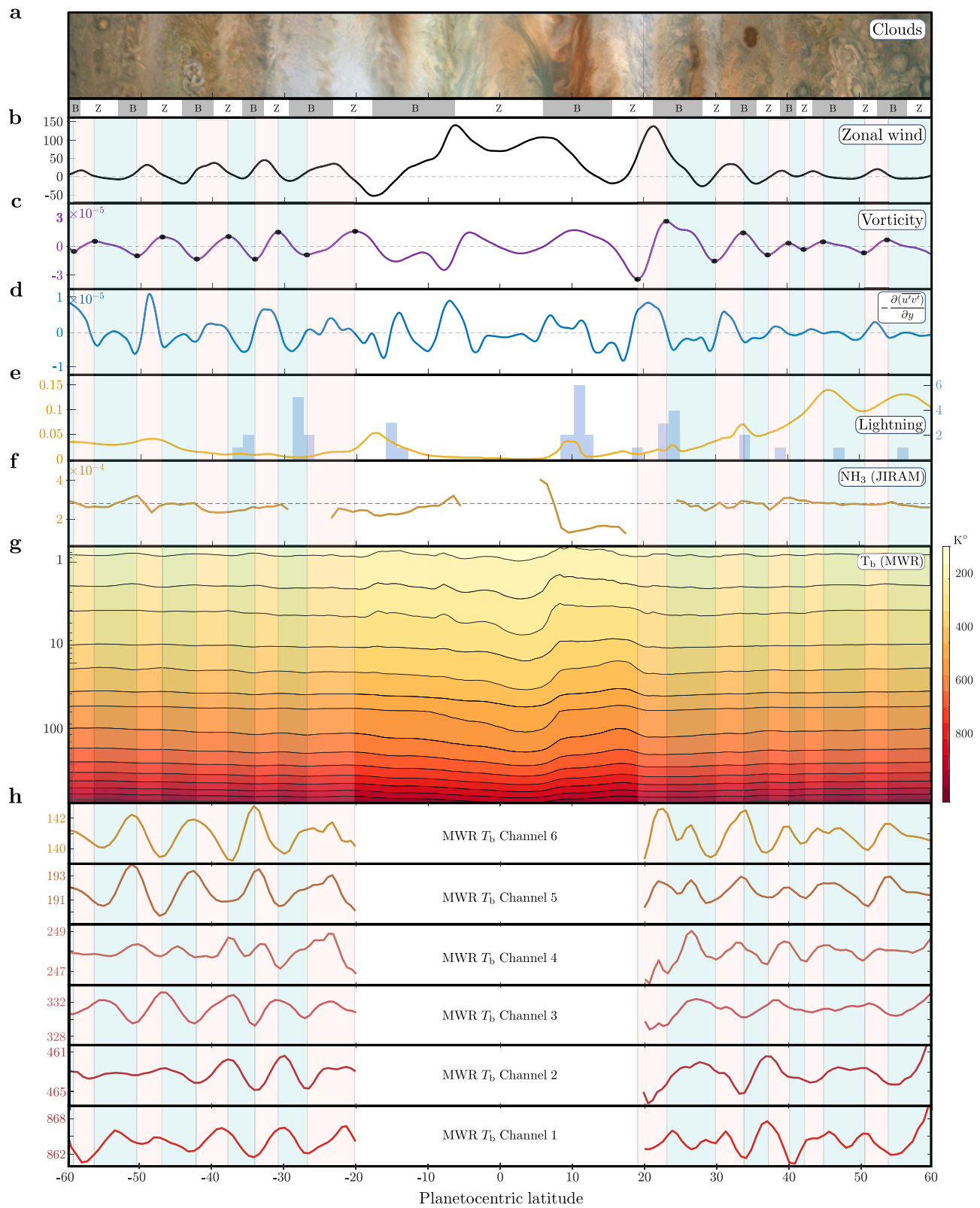


Figure 1.

## 2. Ammonia Anomalies Due to Vertical Advection

In the presence of a stable vertical ammonia concentration gradient, advection by the vertical branches of a meridional circulation can affect the concentration distribution, potentially leading to steady anomalies. Therefore, the wavy structure of Jupiter's ammonia distribution (Figures 1f–1h) can be explained by the presence of meridional circulation cells. On Jupiter, as condensation of ammonia is expected only at the upper levels of the atmosphere (0.5–1 bar), the ammonia concentration at those levels should be lower than at depth (Fletcher et al., 2020). In addition, precipitation, small-scale turbulence, thermochemical and chemical reactions, and diffusion are also expected to determine the vertical ammonia distribution ( $M_a$ ) (Guillot, Stevenson, et al., 2020). The  $M_a$  profile estimated from the MWR (Li et al., 2017) reveals a local minimum at ~6 bar (Figure 2a). This profile is used in this study as the background state, to explain the ammonia anomalies.

Here, we focus on two regions with distinctly different deep dynamics: the equatorial region (planetocentric latitudes 20°S to 20°N), where superrotation is assumed to be fueled by eddy momentum fluxes perpendicular to the spin axis (e.g., Busse, 2002), and the midlatitudes (60°S to 20°S and 20°N to 60°N), where alternating jets are postulated to be driven by horizontal eddies (e.g., Salyk et al., 2006; Schneider & Liu, 2009; Young et al., 2019), associated with mass-transporting meridional cells.

### 2.1. Midlatitudes Ferrel-Like Cells

We begin with the midlatitudes, where the meridional cells are mechanically driven (see below) by turbulence, similar to Earth's Ferrel cells, which form as a consequence of atmospheric waves breaking in midlatitudes (Vallis, 2017). Unlike the largely baroclinic midlatitudes of Earth, which result in mostly nonmass-transporting Ferrel cells (Jukes, 2001; Vallis, 2017), the predominantly barotropic flows on Jupiter (at the depth range associated with the MWR measurements; Galanti & Kaspi, 2021; Kaspi et al., 2018, 2020) may allow mass-transporting meridional cells (see Supporting Information S1). Consistently, deep convection models of Jupiter also show barotropic flows (e.g., Aurnou & Olson, 2001; Busse, 1976). The upper branch of Earth's Ferrel cells consists of a balance between the Coriolis force and the eddy momentum flux convergence

$$-f\bar{v} = -\frac{\partial(\overline{u'v'})}{\partial y}, \quad (1)$$

where  $f$  is the Coriolis parameter. This upper branch balance, which is the leading-order balance of the steady-state zonal-mean zonal momentum equation, is expected to hold within the equivalent cells on Jupiter (see Supporting Information S1). This balance can hold down to a depth of only a few bars, as inferred from energy considerations (Liu & Schneider, 2010), implying flows from belts to zones within the cloud layer of the Jovian atmosphere. In the lower branch of the terrestrial Ferrel cells, the balance is between the Coriolis force and a surface drag (Vallis, 2017). Since the Jovian atmosphere lacks a bottom solid boundary, surface drag cannot act to oppose the Coriolis force, although it has been suggested that if the cells extend as deep as the jets (Kaspi et al., 2020), the Lorentz force can act as a magnetic drag (Liu & Schneider, 2010; Liu et al., 2008; Wicht et al., 2019). Another possible mechanism that allows the jets to be barotropic in the upper atmosphere and decay in the interior is the presence of a stable layer, as was shown lately in several studies (Christensen et al., 2020; Debras & Chabrier, 2019; Wicht & Gastine, 2020).

**Figure 1.** Observations of Jupiter's atmosphere. (a) Image of Jupiter's clouds (longitudes 69–87°) taken by JunoCam on December 26, 2019 during perijove 24 (image credit: NASA/JPL/SwRI/MSSS/Gerald Eichstaedt/John Rogers), with the traditional “dark” belts (“bright” zones) defined as regions of cyclonic (anticyclonic) vorticity, identified below as “B” (“Z”). (b) Jupiter's zonally averaged zonal wind ( $\pm 15 \text{ m s}^{-1}$ ) measured by the Hubble space telescope on December 11, 2016, during Juno's third perijove (Tollefson et al., 2017). (c) The zonally averaged vorticity [ $\text{s}^{-1}$ ], calculated from the zonal wind profile (panel b). Black dots represent local extrema in the midlatitudes. (d) Eddy momentum flux convergence ( $\pm 2 \times 10^{-6} \text{ m s}^{-2}$ ) calculated from 58 image pairs taken by Cassini during its Jupiter flyby in December, 2000 (Salyk et al., 2006). (e) Lightning detections ( $\text{s}^{-1}$ ) by Juno's Microwave Radiometer (MWR) during perijoves 1–8 (yellow, left axis, Brown et al., 2018) and number of lightning storms detected by Cassini during its flyby (blue, right axis, Porco et al., 2003). (f) Distribution of ammonia (volume mixing ratio) and its mean (dashed) at a depth of ~6 bar, measured by Juno's Jovian Infrared Auroral Mapper (JIRAM) during perijoves 1–15 (Grassi et al., 2020). (g) Nadir  $T_b$  (°K) (color) interpolated between pressure levels of 0.7 and 240 bar (vertical axis), measured by Juno's MWR during perijoves 1–12 (Oyafuso et al., 2020). (h) Reconstructed MWR Brightness temperature at midlatitudes. A frequency filter is applied according to Equation S7 in Supporting Information S1. The standard deviation of each channel and latitude is available in Figures S3 and S4 in Supporting Information S1. It can be seen that  $T_b$  changes its trend at the borders between cells, consistent with the Ferrel-like cells hypothesis. (b–h) Light red (blue) bands in the midlatitudes indicate regions of positive (negative) vorticity gradients.

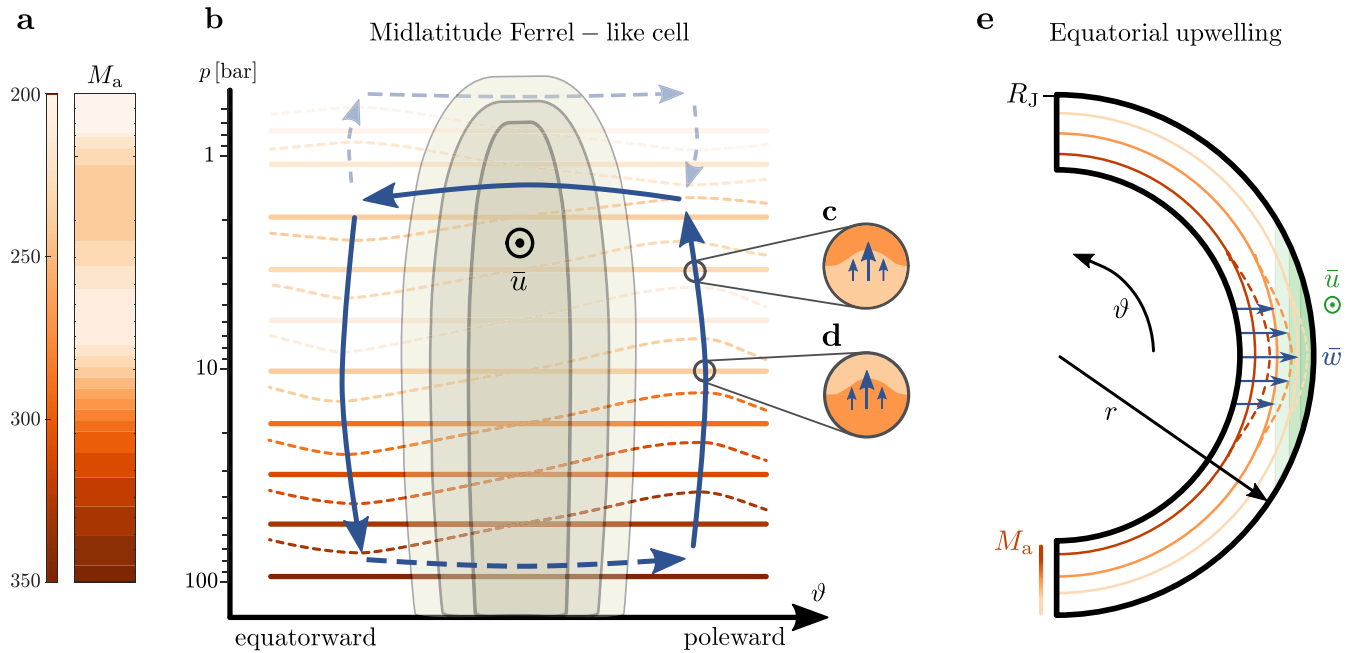


**Figure 2.** Schematics of Jupiter's meridional circulation as inferred from the ammonia distribution. (a) The vertical structure (aligned to the pressure scale at panel b) of the meridionally averaged ammonia concentration ( $M_a$ ) (ppm), as interpreted from the  $T_b$  data (Li et al., 2017). (b) Illustration of a midlatitude Ferrel-like circulation cell (blue arrows) in the northern hemisphere (NH), looking from east toward the west. The cells are accompanied by an eddy-driven barotropic jet ( $\bar{u}$ ), which peaks at the center of the cell (beige contours). Ammonia constant-concentration lines are illustrated with orange shades (according to the ammonia vertical profile from panel a). Dashed orange lines are deviations from  $M_a$ , driven by vertical advection. The return flow of the cell, illustrated by a dashed blue arrow, lies at an unknown depth. An oppositely directed upper cell, as suggested by pre-Juno measurements (Fletcher et al., 2020; Ingersoll et al., 2000; Showman & de Pater, 2005), is demonstrated by dashed transparent arrows.  $p$  is pressure, taken as a vertical coordinate. (c) A closer look at the region where the rising air advects ammonia-poor fluid to an ammonia-rich layer, associated with pressure levels between 1.5 and 6 bar. (d) Here, rising gas drags higher ammonia concentration to a lower ammonia concentration region, associated with pressure levels deeper than 6 bar. (e) A cross section of Jupiter's equatorial upwelling ( $\bar{w}$ ), associated with a superrotating jet ( $\bar{u}$ , green contours), leading to an ammonia concentration maximum. The equatorial  $M_a$  (orange contours) is assumed to decrease with radius (Figure S8 in Supporting Information S1).  $R_J$  is Jupiter's radius and  $\vartheta$  and  $r$  are the latitudinal and radial directions, respectively.

The direction of each Ferrel-like cell corresponds to the direction of the respective midlatitude jet. Eastward (westward) jets are located in cells of eastward momentum flux convergence (divergence) implying (Equation 1) a counterclockwise (clockwise) circulation in the NH, and a clockwise (counterclockwise) circulation in the SH (Figures 1b and 1d; Figure 2b). The upper branch of the Ferrel-like cells may coincide with the lower branch of stacked upper cells with an opposite circulation (Ingersoll et al., 2000; Showman & de Pater, 2005) (dashed transparent lines in Figure 2b), and therefore may share the same balance (Equation 1). Indications for the upper cells come from measurements of temperature and shallow tracer distributions (de Pater et al., 2019; Fletcher et al., 2016; Gierasch et al., 1986). Similar to the balance describing the deeper branch of the lower cells, the upper branch of the upper cells requires a drag force, which may result from breaking of atmospheric waves (Gierasch et al., 1986; Ingersoll et al., 2021).

The background ammonia profile is skewed by the vertical branches of the cells (dashed orange lines in Figure 2b), maximizing the ammonia meridional gradient ( $\partial_y m_a$ ) where the jet velocity peaks (i.e., in the middle of the cell). This means that a correlation (along isobars) is expected between the zonal jets and the meridional gradient of the ammonia concentration at midlatitudes (Duer et al., 2020; Fletcher et al., 2021). However, since the vertical gradient of  $M_a$  changes with depth (Li et al., 2017; Figure 2a), the nature of the correlation should change as well, as illustrated in Figures 2c and 2d. These simple considerations motivate the examination of the correlation between  $\bar{u}$  and  $\partial_y m_a$  ( $-\partial_y T_b$ ) in midlatitudes (Figures 3a and 3c, also see Supporting Information S1). Note that  $T_b$  corresponds inversely to ammonia abundance at a certain pressure level (Li et al., 2017). For a deep-wind estimate, we use the measured cloud-level winds (Tollefson et al., 2017) projected inward in a direction parallel to the axis of rotation, without any change in magnitude (in the upper 240 bar), as implied by gravity measurement constraints (Galanti & Kaspi, 2021; Galanti et al., 2021). The correlations are performed using a  $4^\circ$  latitudinal bin



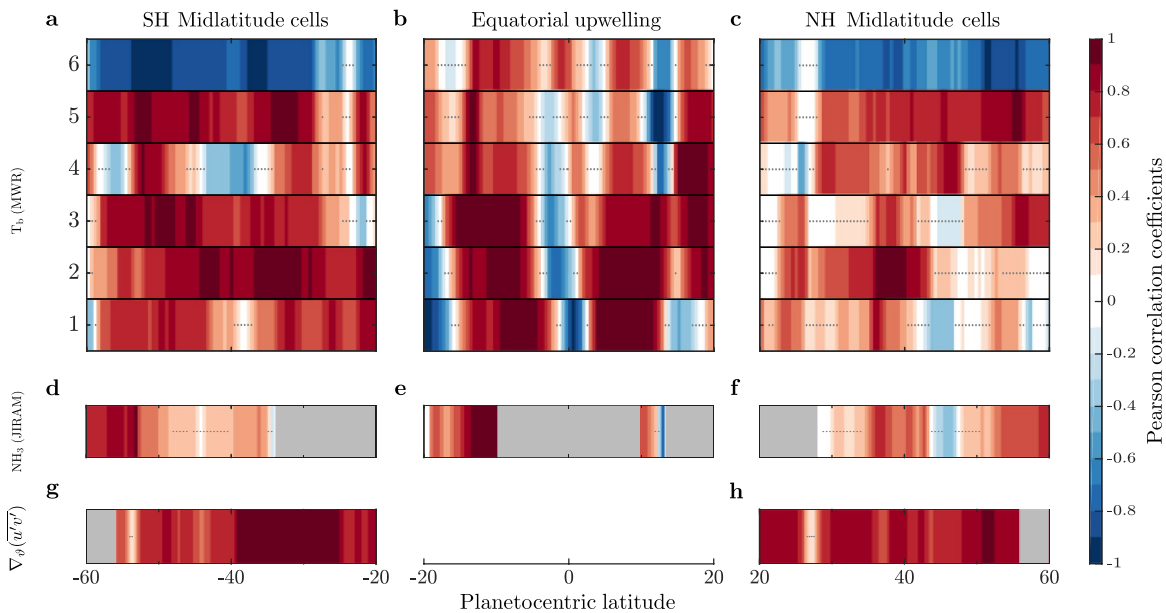


**Figure 3.** Pearson correlation coefficients as a function of latitude (see Supporting Information S1 for details of the calculations). The correlations exemplify the relations presented in Figure 2. (a and c) Correlations calculated between the zonal jets ( $\bar{u}$ ) and the  $T_b$  meridional gradients ( $\partial_y T_b$ ), adjusted by the sign of the vertical gradient of  $M_b$ , in the six Microwave Radiometer (MWR) channels, for the southern hemisphere (SH) and northern hemisphere (NH), respectively. (b) Correlations computed between the zonal jet velocity and  $T_b$  ( $\bar{u} \propto -T_b$ ). (d and f) Correlations between the zonal velocity and the ammonia abundance gradients ( $\partial_y \text{NH}_3$ ), measured by Jovian Infrared Auroral Mapper (JIRAM), in the SH and NH, respectively. (e) Correlations between the zonal velocity and the ammonia abundance from JIRAM ( $\bar{u} \propto \text{NH}_3$ ). (g and h) Correlations between the zonal velocity and the eddy momentum flux convergence ( $\bar{u} \propto -\partial_y(\overline{u'v'})$ ), in the SH and NH, respectively. Gray dots represent correlations that are not statistically significant (confidence level 95%) and gray regions show where measurements were not available. No data are available for the eddy fluxes in the equatorial region, as evaluating them requires measurements of the vertical winds (see Supporting Information S1), which are yet to be achieved.

(see Supporting Information S1). By this, the suggested correlations in Figure 2 can be tested locally, rather than over an entire hemisphere (Duer et al., 2020; Fletcher et al., 2021).

At midlatitudes the overall positive correlations for MWR channels 1–5 indicate the existence of Ferrel-like cells at depths between 1.5 and 240 bar (Figures 3a and 3c). The positive correlation with ammonia estimates by JIRAM (Figures 3d and 3f) further establishes the prominence of the proposed cells. Channel 6 ( $\sim 0.7$  bar) exhibits negative correlations in midlatitudes (Figures 3a and 3c), implying that the deep cells do not extend higher than  $\sim 1$  bar, and supports the existence of counterrotating cells above that level (Fletcher et al., 2020; Ingersoll et al., 2000; Showman & de Pater, 2005). To verify that the relation shown in Equation 1 holds in the cells as illustrated in Figure 2b, regional correlations between  $\bar{u}$  and  $-\partial_y(\overline{u'v'})$  are shown for midlatitudes (Figures 3g and 3h). This positive correlation further strengthens the existence of the Ferrel-like cells, where converging eddy momentum fluxes are the source of momentum. Overall, the correlation analysis reveals multiple deep Ferrel-like cells, extending from  $\sim 1$  bar to at least 240 bar.

## 2.2. Equatorial Upwelling

The equatorial region of Jupiter, characterized by a wide eastward jet, needs to be treated differently. Gravity analysis reveals that Jupiter's interior (deeper than  $\sim 3,000$  km) is rotating as a rigid body (Guillot et al., 2018). Extending the zonal wind along the direction of the spin axis thus separates the equatorial region ( $17^\circ\text{S}$  to  $17^\circ\text{N}$ ) from the truncated cells at midlatitudes (see Supporting Information S1). The superrotating wind at low latitudes requires a source of momentum (Imamura et al., 2020). Theories for such sources include meridional (Laraia & Schneider, 2015; Potter et al., 2014) and vertical (Aurnou & Olson, 2001; Busse, 2002; Christensen, 2002; Dietrich & Jones, 2018; Heimpel et al., 2005; Kaspi et al., 2009), propagation of waves. For the vertical case, several studies have shown that an equatorial superrotation in giant planets can be driven by eddy momentum fluxes perpendicular to the axis of rotation (Gastine et al., 2014; Heimpel et al., 2005; Kaspi et al., 2009). These fluxes transfer momentum outwards and lead to a mean upwelling at the equatorial region (see Supporting

Information S1). Such an upwelling should lead to a maximum concentration anomaly of any stably stratified matter (Figure 2e). In the equatorial region, the minimum in  $M_a$  around  $\sim 6$  bar nearly vanishes (Figure S8 in Supporting Information S1), suggesting that the positive ammonia anomalies at the equatorial region (Figure S2a in Supporting Information S1) are due to the upwelling from deep. To examine this, at the equator, the correlation is calculated between the zonal velocity ( $\bar{u}$ ) and the ammonia concentration itself ( $-T_b$  for the MWR or  $\text{NH}_3$  for the JIRAM measurements). Using a regional correlation analysis (see Supporting Information S1), it is apparent that the correlations are largely positive at all depths (Figures 3b and 3c), implying that an equatorial upwelling is dominant from the cloud-deck and down to at least 240 bar. Very close to the equator, the correlation is negative due to the local minimum in the zonal velocity (Figure 1b).

### 3. Model Reproduction of Jupiter's Ammonia Distribution

To further validate that the positive correlations shown in Figures 3a and 3c are indeed due to the existence of meridional circulation cells, we reproduce the measured variations using a simplified advection-relaxation model. Beginning with a steady-state zonal-mean conservation of species equation for ammonia, assuming that diffusion terms are small, the leading-order balance is

$$\bar{w}(\vartheta, r) \frac{\partial m_a(\vartheta, r)}{\partial r} + \bar{v}(\vartheta, r) \frac{\partial m_a(\vartheta, r)}{r \partial \vartheta} = -G(r) (m_a(\vartheta, r) - M_a(r)), \quad (2)$$

where  $\bar{w}$  is the zonally averaged radial velocity, and  $m_a$ , the variable solved for by the model, is the (zonal-mean) molar fraction of ammonia.  $M_a$  is the ammonia concentration averaged over isobaric surfaces (Figure 2a), and  $G$  is the inverse of a Newtonian relaxation timescale. The two terms on the left-hand side represent advection by the mean circulation, and the right-hand side term is a source term parameterized as a simple Newtonian relaxation of ammonia. This relaxation term is assumed to include all the processes resulting in the observed  $M_a$  as it acts against local anomalies toward this mean vertical structure. To qualitatively illustrate how the Ferrel-like cells' footprint might appear in the ammonia distribution map ( $m_a$ ), we solve the advection-relaxation balance shown in Equation 2, for the midlatitudes between 1.5 and 240 bar (see Supporting Information S1). As the balance in Equation 2 indicates, it is assumed that the relaxation time scale ( $G^{-1}$ ) is such that the advection and relaxation terms balance each other.

The zonally averaged velocity components ( $\bar{v}$ ,  $\bar{w}$ ) of the circulation cells, necessary for setting the advection terms of Equation 2, can be projected from the available wind data according to the outline illustrated in Figure 2b. Specifically, we relate between the circulation cells and the wind data corresponding to the following assumptions (see also Supporting Information S1). The borders between the cells are set at local extrema of the observed cloud-level vorticity, the directions of the circulation cells are set according to the directions of the jets in the middle of each cell, and the strength of the circulation in each cell is set by the measured eddy momentum flux convergence along the cell (Figure S5 in Supporting Information S1). As the three terms in Equation 2 should be proportional, but cannot be uniquely determined, the values of  $\bar{w}$ ,  $\bar{v}$ , and  $G$  are normalized (Figure 4a). This normalization means that while the model cannot produce absolute values of winds due to unmeasured quantities, it can predict qualitatively how these velocities would be structured spatially and what should be their relative magnitudes, which are sufficient for assessing the existence of the cells. Using scaling arguments, the value of Jupiter's static stability has recently been estimated to be in the order of  $10^{-2} \text{ s}^{-1}$  (Lee & Kaspi, 2021), which can provide a further step toward estimating the magnitude of the velocities in the cells.

The described wind scheme results in upwellings (downwellings) on the poleward (equatorward) sides of eastward jets (Figure 4a). The cells are reversed for westward jets. Finally, as a benchmark for the model results, derivation of the ammonia abundance ( $m_a^{(\text{data})}$ ) from the measured  $T_b$  between the latitudes  $60^\circ\text{S}$  and  $60^\circ\text{N}$  is implemented (see Figure S2 in Supporting Information S1). As the depth of the cells, the width of their branches and the parameter  $G$  are unknown, an optimization procedure is performed for determining these parameters to best match the data (see Supporting Information S1). To ensure that this procedure does not influence the qualitative nature of the results, Equation 2 is also solved with a predefined physically oriented set of parameters (Figures S6 and S7 in Supporting Information S1).

Using the above assumptions, we solve Equation 2 to predict the ammonia map ( $m_a^{(\text{model})}$ ), and compare it to  $m_a^{(\text{data})}$  (Figure 4). We stress that the latitudinal variations appearing in the results (Figure 4c), stem only from

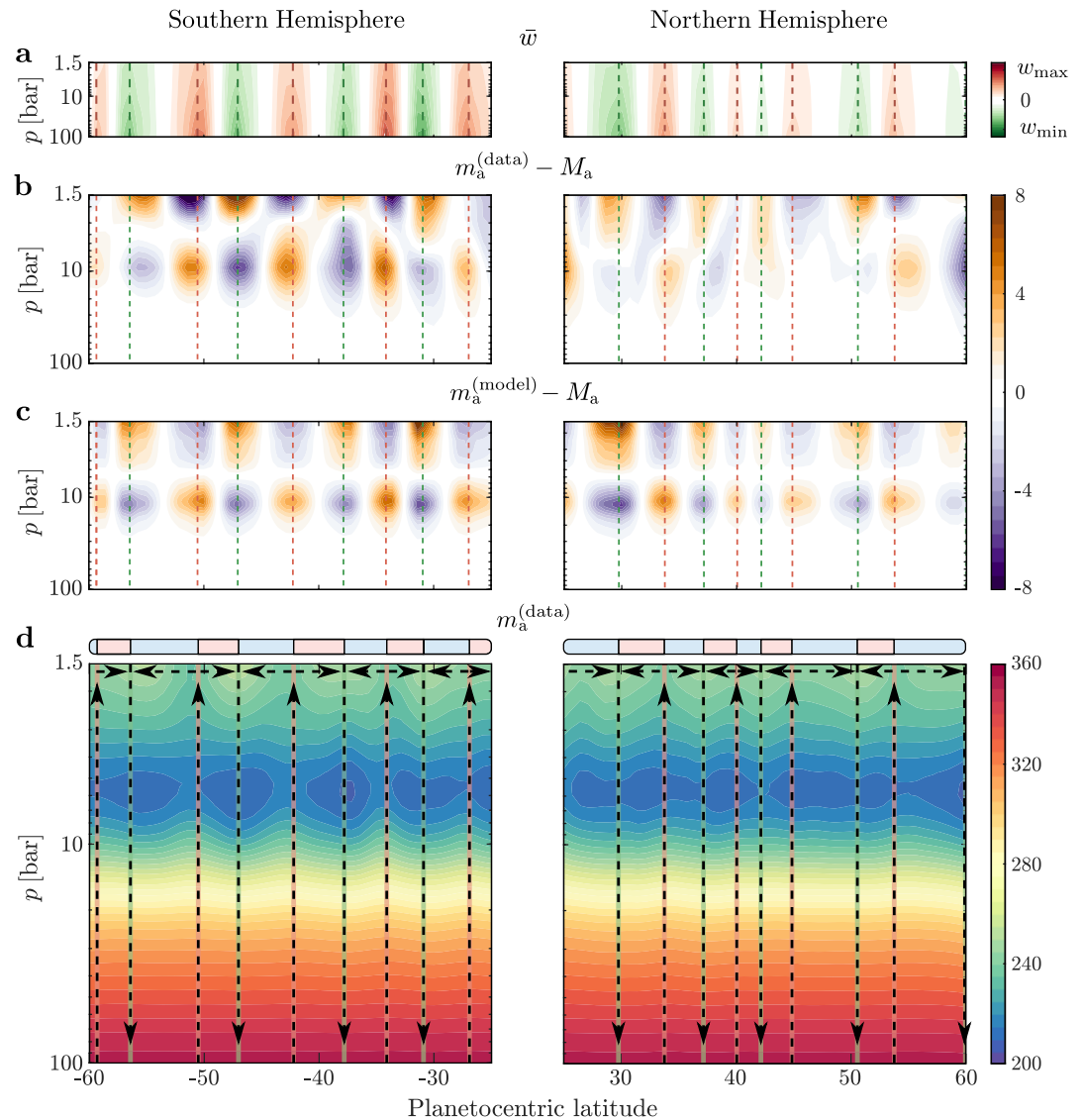


**Figure 4.** Jupiter's ammonia distribution driven by an array of circulation cells. (a) The normalized vertical zonal-mean wind ( $\bar{w}$ ), as a function of latitude and pressure, used in the model. Red and green contours are upward and downward winds, respectively. (b) The ammonia anomalies reconstructed from the data (ppm). Here, the vertical mean profile  $M_a$  is removed from the ammonia map  $m_a$ . (c) The ammonia anomalies (ppm) produced by the advection-relaxation model. (d) The full reconstructed ammonia map  $m_a^{(data)}$  (ppm). Arrows represent the direction of the cells' vertical and meridional winds. (a)–(d) Red and green vertical lines are the locations of the upward and downward branches of the cells, respectively. For reference, light red (blue) bands indicate regions of positive (negative) vorticity gradient as in Figure 1. The vertical axis is truncated at 100 bar as  $M_a$  becomes largely uniform beyond this depth, thereby suppressing footprints of advection.

the cloud-level wind observations without any assumption on the meridional ammonia variation. For a clear comparison between the  $m_a^{(data)}$  and  $m_a^{(model)}$ ,  $M_a$  is subtracted from both, such that only anomalies are visible (Figures 4b and 4c). Around 10 bar (Figure 4b), where  $M_a$  greatly increases with depth, enriched (depleted) ammonia anomalies appear where upwellings (downwellings) are expected (Figure 4a). These features flip sign around the 6-bar level, where  $M_a$  decreases with depth. These elements are captured well by the advection-relaxation model (Figure 4c). In the SH, all 18 anomalies apparent in the observations have a counterpart of similar sign, shape and position in the model results, suggesting the existence of eight meridional circulation cells. This agreement validates that advection by the vertical branches of the cells is the main contributor in the creation of the observed ammonia anomalies. In the NH, similar results are achieved, although the cells are slightly less coherent, perhaps due to unexplained differences between the perijoves in the NH midlatitudes (Figure S3 in Supporting



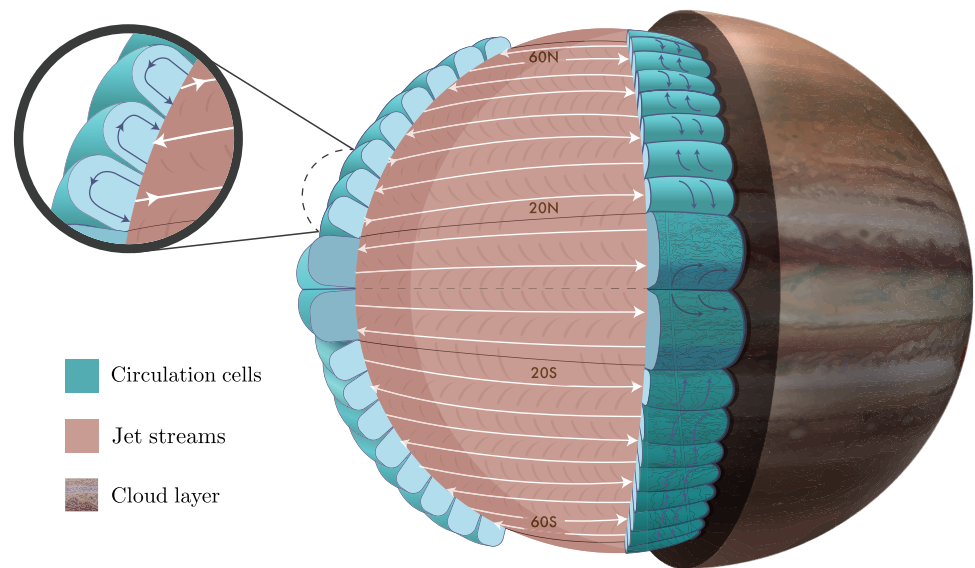


**Figure 5.** A figurative cross section of Jupiter's meridional circulation and a magnification of the midlatitude circulation cells. The circulation cells (blue) are axisymmetric in the zonal direction. The pink shell represents a deep layer characteristic for all depths within the circulation cells. The white arrows represent alternating jet streams and are symmetric around the equator for the purpose of clarity. Each jet between latitudes  $20^{\circ} - 60^{\circ}\text{N/S}$  is accompanied by a turbulence-driven circulation cell (blue arrows) in the meridional plane as illustrated in Figure 2b. The equatorial upwelling associated with the superrotating jet is drawn at the equator, as part of a larger possible equatorial cell (dark blue).

Information S1; Fletcher et al., 2021; Oyafuso et al., 2020), which might mask the cells' footprints in the MWR data. Nevertheless, the lightning data reinforces the existence of the NH cells, as lightning peaks are aligned with the rising branch of the cells at the poleward side of the eastward jets (Figures 1e and S1 in Supporting Information S1), which combined with the MWR data (Figures 4b–4d) provide indication for eight northern cells. Additional NH centered perijoves during the Juno extended mission may provide data to better constrain the NH cells. For more intuition, one can look at the full ammonia map (Figure 4d), where iso-concentration lines are pulled up and down by the vertical winds (as schematically illustrated in Figure 2b), emphasizing the locations of the 16 eddy-driven cells evident in the MWR data.

#### 4. Discussion

The identified array of alternating cells in midlatitudes, along with the equatorial upwelling, are key features in the meridional overturning circulation of the Jovian atmosphere (Figure 5). The cells' depth that can be inferred from the MWR measurements is limited to the sensing range ( $\sim 240$  bar), but they are likely to extend deeper into the planet, as suggested by multiple theoretical studies (e.g., Christensen et al., 2020; Liu & Schneider, 2010). Another example for deep, turbulence driven, meridional circulation cells may exist on the sun (Miesch & Hindman, 2011).

This study provides an explanation for the observed meridional ammonia anomalies, given the meridionally averaged vertical ammonia profile. The consistency of these results suggest that the  $T_b$  latitudinal variations are dominated by the opacity of a passive tracer, rather than the kinetic temperature. Note that evidence for the part of the deep cells extending from 1.5 to 6 bar depends on the flip of the background ammonia vertical gradient (Figure 2a), and without it these depths might be part of upper inverse cells (Fletcher et al., 2021). The shape of this vertical profile might be set by precipitation, diffusion, and small-scale mixing, all of which might change with latitude and depth (Guillot, Li, et al., 2020). Nonetheless, the remarkable agreement between the model and the data, together with the robust correlation analysis, provide strong evidence that the observed distribution of ammonia is governed by the existence, number, position, and relative strength of the Ferrel-like circulation cells in Jupiter.

## Data Availability Statement

All the data used in this study are publicly available, see Tollefson et al. (2017) for the winds data, Salyk et al. (2006) for the eddies data, Li et al. (2017) for the ammonia data, Brown et al. (2018) for the lightning data, and Oyafuso et al. (2020) for the brightness temperature data.

## Acknowledgments

Keren Duer, Nimrod Gavriel, Eli Galanti and Yohai Kaspi are supported by the Israeli Space Agency and the Helen Kimmel Center for Planetary Science at the Weizmann Institute of Science. Leigh N. Fletcher was supported by a European Research Council Consolidator Grant (under the European Union's Horizon 2020 research and innovation programme, grant agreement no 723890) at the University of Leicester. Davide Grassi is supported by the Italian Space Agency through ASI-INAFA contract 2016-23-H.1-2018. Some of this research was carried out at the Jet Propulsion Laboratory, California Institute of Technology, under a contract with the National Aeronautics and Space Administration (80NM0018D0004). All authors have been supported by the Juno project.

## References

- Aurnou, J. M., & Olson, P. L. (2001). Strong zonal winds from thermal convection in a rotating spherical shell. *Geophysical Research Letters*, 28(13), 2557–2559. <https://doi.org/10.1029/2000GL012474>
- Bolton, S. J., Adriani, A., Adamitroaie, V., Allison, M., Anderson, J., Atreya, S., et al. (2017). Jupiter's interior and deep atmosphere: The initial pole-to-pole passes with the Juno spacecraft. *Science*, 356, 821–825. <https://doi.org/10.1126/science.aal2108>
- Brown, S., Janssen, M., Adamitroaie, V., Atreya, S., Bolton, S., Gulkis, S., et al. (2018). Prevalent lightning sferics at 600 megahertz near Jupiter's poles. *Nature*, 558(7708), 87–90. <https://doi.org/10.1038/s41586-018-0156-5>
- Busse, F. H. (1976). A simple model of convection in the Jovian atmosphere. *Icarus*, 29, 255–260. [https://doi.org/10.1016/0019-1035\(76\)90053-1](https://doi.org/10.1016/0019-1035(76)90053-1)
- Busse, F. H. (2002). Convective flows in rapidly rotating spheres and their dynamo action. *Physics of Fluids*, 14, 1301–1314. <https://doi.org/10.1063/1.1455626>
- Christensen, U. R. (2002). Zonal flow driven by strongly supercritical convection in rotating spherical shells. *Journal of Computational Physics*, 170, 115–133. <https://doi.org/10.1017/s0022112002002008>
- Christensen, U. R., Wicht, J., & Dietrich, W. (2020). Mechanisms for limiting the depth of zonal winds in the gas giant planets. *The Astrophysical Journal*, 890(1), 61. <https://doi.org/10.3847/1538-4357/ab698c>
- Debras, F., & Chabrier, G. (2019). New models of Jupiter in the context of Juno and Galileo. *The Astrophysical Journal*, 872(1), 100. <https://doi.org/10.3847/1538-4357/aaff65>
- de Pater, I., Dunn, D., Romani, P., & Zahnle, K. (2001). Reconciling Galileo probe data and ground-based radio observations of ammonia on Jupiter. *Icarus*, 149(1), 66–78. <https://doi.org/10.1006/icar.2000.6527>
- de Pater, I., Sault, R. J., Wong, M. H., Fletcher, L. N., DeBoer, D., & Butler, B. (2019). Jupiter's ammonia distribution derived from VLA maps at 3–37 GHz. *Icarus*, 322, 168–191. <https://doi.org/10.1016/j.icarus.2018.11.024>
- Dietrich, W., & Jones, C. A. (2018). Anelastic spherical dynamos with radially variable electrical conductivity. *Icarus*, 305, 15–32. <https://doi.org/10.1016/j.icarus.2018.01.003>
- Duer, K., Galanti, E., & Kaspi, Y. (2020). The range of Jupiter's flow structures that fit the Juno asymmetric gravity measurements. *Journal of Geophysical Research: Planets*, 125, e2019JE006292. <https://doi.org/10.1029/2019JE006292>
- Fletcher, L. N., Greathouse, T. K., Orton, G. S., Sinclair, J. A., Giles, R. S., Irwin, P. G., & Encenaz, T. (2016). Mid-infrared mapping of Jupiter's temperatures, aerosol opacity and chemical distributions with IRTF/TEXES. *Icarus*, 278, 128–161. <https://doi.org/10.1016/j.icarus.2016.06.008>
- Fletcher, L. N., Kaspi, Y., Guillot, T., & Showman, A. P. (2020). How well do we understand the belt/zone circulation of Giant Planet atmospheres? *Space Science Reviews*, 216(2), 30. <https://doi.org/10.1007/s11214-019-0631-9>
- Fletcher, L. N., Oyafuso, F. A., Allison, M., Ingersoll, A., Li, L., Kaspi, Y., et al. (2021). Jupiter's temperate belt/zone contrasts revealed at depth by Juno microwave observations. *Journal of Geophysical Research: Planets*, 126(10). <https://doi.org/10.1029/2021JE006858>
- Galanti, E., & Kaspi, Y. (2021). Combined magnetic and gravity measurements probe the deep zonal flows of the gas giants. *Monthly Notices of the Royal Astronomical Society*, 501(2), 2352–2362. <https://doi.org/10.1093/mnras/staa3722>
- Galanti, E., Kaspi, Y., Duer, K., Fletcher, L. N., Ingersoll, A., Cheng, L., et al. (2021). Constraints on the latitudinal profile of Jupiter's deep jets. *Geophysical Research Letters*, 48, e2021GL092912. <https://doi.org/10.1029/2021GL092912>
- Garcia-Melendo, E., & Sánchez-Lavega, A. (2001). A study of the stability of Jovian zonal winds from HST images: 1995–2000. *Icarus*, 152(2), 316–330. <https://doi.org/10.1006/icar.2001.6646>
- Gastine, T., Wicht, J., Duarte, L. D. V., Heimpel, M., & Becker, A. (2014). Explaining Jupiter's magnetic field and equatorial jet dynamics. *Geophysical Research Letters*, 41, 5410–5419. <https://doi.org/10.1002/2014GL060814>
- Gierasch, P. J., Magalhaes, J. A., & Conrath, B. J. (1986). Zonal mean properties of Jupiter's upper troposphere from Voyager infrared observations. *Icarus*, 67, 456–483. [https://doi.org/10.1016/0019-1035\(86\)90125-9](https://doi.org/10.1016/0019-1035(86)90125-9)
- Giles, R. S., Fletcher, L. N., Irwin, P. G., Orton, G. S., & Sinclair, J. A. (2017). Ammonia in Jupiter's troposphere from high-resolution 5  $\mu$ m spectroscopy. *Geophysical Research Letters*, 44, 10838–10844. <https://doi.org/10.1002/2017GL075221>
- Grassi, D., Adriani, A., Moriconi, M. L., Ignatiev, N. I., D'Aversa, E., Colosimo, F., et al. (2010). Jupiter's hot spots: Quantitative assessment of the retrieval capabilities of future IR spectro-imagers. *Planetary and Space Science*, 58(10), 1265–1278. <https://doi.org/10.1016/j.pss.2010.05.003>
- Grassi, D., Adriani, A., Mura, A., Atreya, S. K., Fletcher, L. N., Lunine, J. I., & Turrini, D. (2020). On the spatial distribution of minor species in Jupiter's troposphere as inferred from Juno JIRAM data. *Journal of Geophysical Research: Planets*, 125, e2019JE006206. <https://doi.org/10.1029/2019JE006206>
- Guillot, T., Li, C., Bolton, S. J., Brown, S. T., Ingersoll, A. P., Janssen, M. A., & Stevenson, D. J. (2020). Storms and the depletion of ammonia in Jupiter: II. Explaining the Juno observations. *Journal of Geophysical Research: Planets*, 125, e2020JE006404. <https://doi.org/10.1029/2020JE006404>
- Guillot, T., Miguel, Y., Militzer, B., Hubbard, W. B., Kaspi, Y., Galanti, E., et al. (2018). A suppression of differential rotation in Jupiter's deep interior. *Nature*, 555, 227–230. <https://doi.org/10.1038/nature25775>
- Guillot, T., Stevenson, D. J., Atreya, S. K., Bolton, S. J., & Becker, H. N. (2020). Storms and the depletion of ammonia in Jupiter: I. Microphysics of mush balls. *Journal of Geophysical Research: Planets*, 125, e2020JE006403. <https://doi.org/10.1029/2020JE006403>
- Heimpel, M., Aurnou, J., & Wicht, J. (2005). Simulation of equatorial and high-latitude jets on Jupiter in a deep convection model. *Nature*, 438, 193–196. <https://doi.org/10.1038/nature04208>
- Iess, L., Folkner, W. M., Durante, D., Parisi, M., Kaspi, Y., Galanti, E., et al. (2018). Measurement of Jupiter's asymmetric gravity field. *Nature*, 555(7695), 220–222. <https://doi.org/10.1038/nature25776>
- Imamura, T., Mitchell, J., Lebonnois, S., Kaspi, Y., Showman, A. P., & Korabely, O. (2020). Superrotation in planetary atmospheres. *Space Science Reviews*, 216(5), 87. <https://doi.org/10.1007/s11214-020-00703-9>

- Ingersoll, A. P., Adumitroaie, V., Allison, M. D., Atreya, S., Bellotti, A. A., Bolton, S. J., et al. (2017). Implications of the ammonia distribution on Jupiter from 1 to 100 bars as measured by the Juno microwave radiometer. *Geophysical Research Letters*, 44, 7676–7685. <https://doi.org/10.1002/2017GL074277>
- Ingersoll, A. P., Atreya, S., Bolton, S. J., Brueschaber, S., Fletcher, L. N., Galanti, E., & Waite, H. (2021). Jupiter's overturning circulation: Breaking waves take the place of solid boundaries. *Geophysical Research Letters*, 48. <https://doi.org/10.1029/2021GL095756>
- Ingersoll, A. P., Gierasch, P. J., Banfield, D., Vasavada, A. R., & Galileo Imaging Team. (2000). Moist convection as an energy source for the large-scale motions in Jupiter's atmosphere. *Nature*, 403, 630–632. <https://doi.org/10.1038/35001021>
- Janssen, M. A., Oswald, J. E., Brown, S. T., Gulkis, S., Levin, S. M., Bolton, S. J., et al. (2017). MWR: Microwave radiometer for the Juno mission to Jupiter. *Space Science Reviews*, 213(1–4), 139–185. <https://doi.org/10.1007/s11214-017-0349-5>
- Juckes, M. (2001). A generalization of the transformed Eulerian-mean meridional circulation. *Quarterly Journal of the Royal Meteorological Society*, 127(571), 147–160. <https://doi.org/10.1002/qj.49712757109>
- Kaspi, Y., Flierl, G. R., & Showman, A. P. (2009). The deep wind structure of the giant planets: Results from an anelastic general circulation model. *Icarus*, 202, 525–542. <https://doi.org/10.1016/j.icarus.2009.03.026>
- Kaspi, Y., Galanti, E., Hubbard, W. B., Stevenson, D. J., Bolton, S. J., Iess, L., et al. (2018). Jupiter's atmospheric jet-streams extend thousands of kilometres deep. *Nature*, 555, 223–226. <https://doi.org/10.1038/nature25793>
- Kaspi, Y., Galanti, E., Showman, A. P., Stevenson, D. J., Guillot, T., Iess, L., & Bolton, S. J. (2020). Comparison of the deep atmospheric dynamics of Jupiter and Saturn in light of the Juno and Cassini gravity measurements. *Space Science Reviews*, 216(5), 84. <https://doi.org/10.1007/s11214-020-00705-7>
- Laraia, A. L., & Schneider, T. (2015). Superrotation in terrestrial atmospheres. *Journal of the Atmospheric Sciences*, 72(11), 4281–4296. <https://doi.org/10.1175/jas-d-15-0030.1>
- Lee, S., & Kaspi, Y. (2021). Towards an understanding of the structure of Jupiter's atmosphere using the ammonia distribution and the Transformed Eulerian mean theory. *Journal of the Atmospheric Sciences*, 78(7), 2047–2056. <https://doi.org/10.1175/jas-d-20-0342.1>
- Lewis, S. R., Read, P. L., Conrath, B. J., Pearl, J. C., & Smith, M. D. (2007). Assimilation of thermal emission spectrometer atmospheric data during the Mars Global Surveyor aerobraking period. *Icarus*, 192(2), 327–347. <https://doi.org/10.1016/j.icarus.2007.08.009>
- Li, C., Ingersoll, A., Bolton, S., Levin, S., Janssen, M., Atreya, S., et al. (2020). The water abundance in Jupiter's equatorial zone. *Nature Astronomy*, 4(6), 609–616. <https://doi.org/10.1038/s41550-020-1009-3>
- Li, C., Ingersoll, A., Janssen, M., Levin, S., Bolton, S., Adumitroaie, V., et al. (2017). The distribution of ammonia on Jupiter from a preliminary inversion of Juno microwave radiometer data. *Geophysical Research Letters*, 44, 5317–5325. <https://doi.org/10.1002/2017GL073159>
- Limaye, S. S. (2007). Venus atmospheric circulation: Known and unknown. *Journal of Geophysical Research*, 112, E04S09. <https://doi.org/10.1029/2006JE002814>
- Little, B., Anger, C. D., Ingersoll, A. P., Vasavada, A. R., Senske, D. A., Breneman, H. H., & Team, T. G. S. (1999). Galileo images of lightning on Jupiter. *Icarus*, 142(2), 306–323. <https://doi.org/10.1006/icar.1999.6195>
- Liu, J., Goldreich, P. M., & Stevenson, D. J. (2008). Constraints on deep-seated zonal winds inside Jupiter and Saturn. *Icarus*, 196, 653–664. <https://doi.org/10.1016/j.icarus.2007.11.036>
- Liu, J., & Schneider, T. (2010). Mechanisms of jet formation on the giant planets. *Journal of the Atmospheric Sciences*, 67, 3652–3672. <https://doi.org/10.1175/2010JAS3492.1>
- Miesch, M. S., & Hindman, B. W. (2011). Gyroscopic pumping in the solar near-surface shear layer. *The Astrophysical Journal*, 743(1), 79. <https://doi.org/10.1088/0004-637x/743/1/79>
- Oyafuso, F., Levin, S., Orton, G., Brown, S., Adumitroaie, V., Janssen, M., et al. (2020). Angular dependence and spatial distribution of Jupiter's centimeter-wave thermal emission from Juno's microwave radiometer. *Earth and Planetary Science Letters*, 7, e2020EA001254. <https://doi.org/10.1029/2020EA001254>
- Porco, C. C., West, R. A., McEwen, A., Del Genio, A. D., Ingersoll, A. P., Thomas, P., & Vasavada, A. R. (2003). Cassini imaging of Jupiter's atmosphere, satellites and rings. *Science*, 299, 1541–1547. <https://doi.org/10.1126/science.1079462>
- Potter, S. F., Vallis, G. K., & Mitchell, J. L. (2014). Spontaneous superrotation and the role of Kelvin waves in an idealized dry GCM. *Journal of the Atmospheric Sciences*, 71(2), 596–614. <https://doi.org/10.1175/jas-d-13-0150.1>
- Read, P. L., Lewis, S. R., & Vallis, G. K. (2018). Atmospheric dynamics of terrestrial planets. *Handbook of Exoplanets*, 144, 2537–2557. [https://doi.org/10.1007/978-3-319-30648-3\\_50-2](https://doi.org/10.1007/978-3-319-30648-3_50-2)
- Salyk, C., Ingersoll, A. P., Lorre, J., Vasavada, A., & Del Genio, A. D. (2006). Interaction between eddies and mean flow in Jupiter's atmosphere: Analysis of Cassini imaging data. *Icarus*, 185, 430–442. <https://doi.org/10.1016/j.icarus.2006.08.007>
- Schneider, T. (2006). The general circulation of the atmosphere. *Annual Review of Earth and Planetary Sciences*, 34, 655–688. <https://doi.org/10.1146/annurev.earth.34.031405.125144>
- Schneider, T., & Liu, J. (2009). Formation of jets and equatorial superrotation on Jupiter. *Journal of the Atmospheric Sciences*, 66, 579–601. <https://doi.org/10.1175/2008JAS2798.1>
- Showman, A. P., & de Pater, I. (2005). Dynamical implications of Jupiter's tropospheric ammonia abundance. *Icarus*, 174, 192–204. <https://doi.org/10.1016/j.icarus.2004.10.004>
- Taylor, F. W., Atreya, S. K., Encrenaz, T. H., Hunten, D. M., Irwin, P. G., & Owen, T. C. (2004). *Jupiter: The planet, satellites and magnetosphere* (pp. 59–78). Cambridge University Press.
- Tollefson, J., Wong, M. H., de Pater, I., Simon, A. A., Orton, G. S., Rogers, J. H., et al. (2017). Changes in Jupiter's zonal wind profile preceding and during the Juno mission. *Icarus*, 296, 163–178. <https://doi.org/10.1016/j.icarus.2017.06.007>
- Vallis, G. K. (2017). *Atmospheric and oceanic fluid dynamics* (2nd ed., p. 770). Cambridge University Press.
- Vasavada, A. R., & Showman, A. P. (2005). Jovian atmospheric dynamics: An update after Galileo and Cassini. *Reports on Progress in Physics*, 68, 1935–1996. <https://doi.org/10.1088/0034-4885/68/8/r06>
- Wicht, J., & Gastine, T. (2020). Numerical simulations help revealing the dynamics underneath the clouds of Jupiter. *Nature Communications*, 11(1), 2886. <https://doi.org/10.1038/s41467-020-16680-0>
- Wicht, J., Gastine, T., Duarte, L. D., & Dietrich, W. (2019). Dynamo action of the zonal winds in Jupiter. *Astronomy and Astrophysics*, 629, A125. <https://doi.org/10.1051/0004-6361/201935682>
- Young, R. M., & Read, P. L. (2017). Forward and inverse kinetic energy cascades in Jupiter's turbulent weather layer. *Nature Physics*, 13(11), 1135–1140. <https://doi.org/10.1038/nphys4227>
- Young, R. M., Read, P. L., & Wang, Y. (2019). Simulating Jupiter's weather layer. Part I: Jet spin-up in a dry atmosphere. *Icarus*, 326, 225–252. <https://doi.org/10.1016/j.icarus.2018.12.005>